High Dynamic Control of a Three-Level Voltage Source Converter Drive with Synchronous Motor and Active Front End

Joachim Böcker
DaimlerChrysler AG
Neuendorfstrasse 20A
D-16761 Hennigsdorf, Germany
Phone/Fax +49 3302 8881 30/15
joachim.boecker@daimlerchrysler.com

Jörg Janning and Helmut Jebenstreit
Alstom Power Conversion GmbH
Culemeyerstrasse 1
D-12277 Berlin, Germany
+49 30 7622 2398/2303, +49 30 7622 2370/2303
joerg.janning@powerconv.alstom.com
helmut.jebenstreit@powerconv.alstom.com

Keywords

Adjustable speed drives, converter control, drives, highly dynamic drives, industrial applications, multilevel converters, variable speed drives, vector control.

Abstract

A high dynamic control system for the Alspa VDM 7000 medium voltage drive was implemented, which provides fast torque response times of a few milliseconds despite the typically low switching frequency of GTO thyristors that is necessary to achieve high efficiency. The drive system consists of a three-level voltage source converter with active front-end and a synchronous motor. The drive has most recently been applied for a main strip mill. It provides a maximum of 8.3 MW mechanical power with a rated motor voltage of 3 kV.

Besides motor torque as the main control objective, the control system has to comply with a number of additional objectives and constraints like DC link voltage regulation and balancing, current and torque harmonics, motor flux and excitation.

Introduction

The medium voltage drive Alspa VDM 7000 consists of a three-level voltage source converter. In the current application for a main strip mill the converter is equipped with an active front-end, so that identical converter modules are employed on both the motor and the line sides, Fig. 1 and Fig. 2. The converter feeds a separately excited synchronous motor. The drive system is designed for a maximal mechanical power of 8.3 MW. The rated and maximum frequencies of the motor are 18.3 Hz and 41.3 Hz, resp., i. e. a flux weakening range of 1:2.3. The excitation circuit is fed by a conventional phase-controlled rectifier bridge.

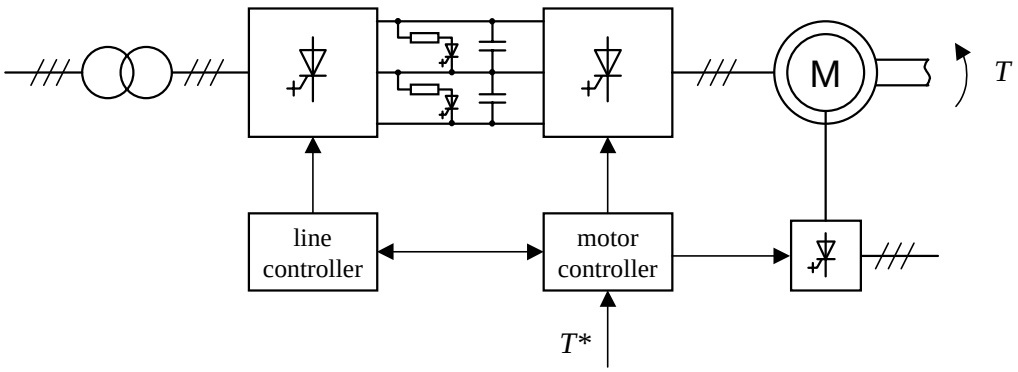

Fig. 1: Basic drive structure.

The main control objective of the converter control is the motor torque *T*, which is demanded by the rolling mill process control that is not a subject of this paper. Besides the motor torque, the converter control design has to take into account a number of additional objectives and constraints such as

- maximum converter currents
- maximum switching frequency
- regulation and balancing of the DC link voltages
- harmonics of line and motor currents and of the motor torque
- control of active and reactive power of line and motor
- excitation of the synchronous motor

The converter control system is split in two main parts, which can be assigned to the two converter units of line and motor as already depicted in Fig. 1.

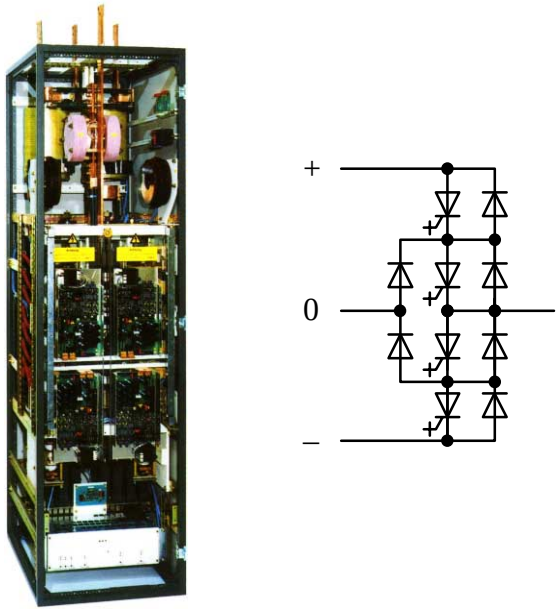

Fig. 2 : Three level GTO converter module. Each of the line and the motor side converters consists of three such modules.

Line-Side Control

Main task of the line-side part of the control system is to regulate the DC link voltages. The DC link controller calculates the demand for an appropriate active line current, Fig. 3. The cascaded inner controller operates in orthogonal components of a rotating *d/q* reference frame which is determined by the line voltage vector. In the context of line-side control, the *q* axis denotes the direction of the line voltage, the *d* axis is orthogonal to it. A power factor controller demands a suitable reactive current component. For better performance, a phase-locked loop (PLL) is applied to track the line voltage vector.

The line-side control is similar to that of a three-level back-to-back converter described earlier in [1], [2] and [3], so that more room should be given to the motor control. Some details of the line-side control, such as the current controller, pulse width modulation (PWM) and DC link balancing are similar or even identical to those of the motor control described below.

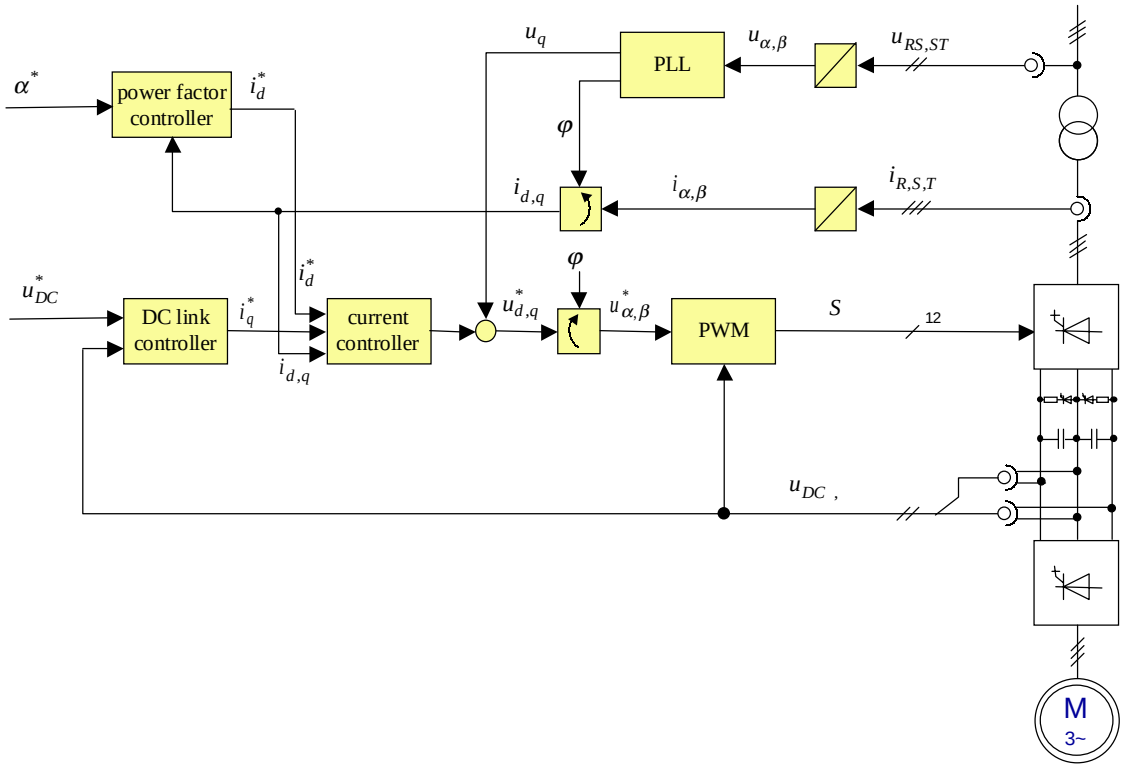

Fig. 3: Line-side control structure.

Motor-Side Control

Motor Model

For a better understanding of the motor control strategy, the following reference frames should be defined first, see Fig. 4. The α/β reference frame is stator-fixed, where the α axis is the direction of phase *R*. The *d/q* frame is aligned with the rotor, where the *d* axis is the direction of the excitation winding.

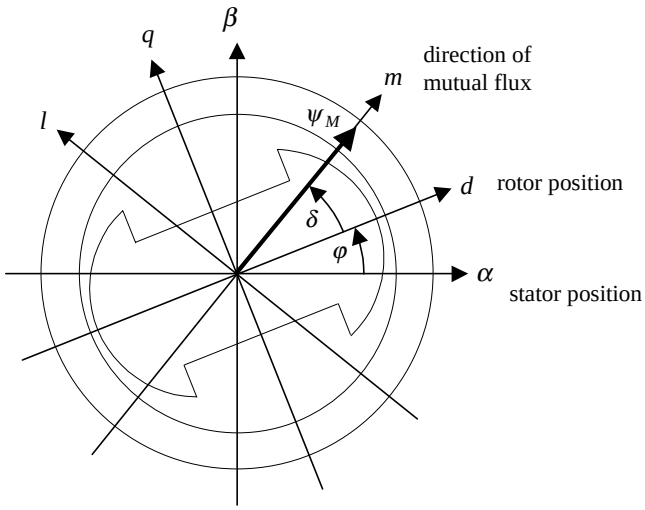

Fig. 4: Reference frames.

The motor model used for the control design is shown in Fig. 5. It consists of a common mutual inductance and independent leakage inductances of the stator, the damper and the excitation circuits.

That is, of course, a rather simple model. In reality, many additional effects as, for example, couplings between damper and excitation circuits, are imaginable. However, it would be a non-trivial task to determine the parameter values of a more complicated model. Last not least, it is good engineering practice to use the simplest possible model for the control *design* while controller *verification* and *validation* should be done with the most comprehensive model that is available.

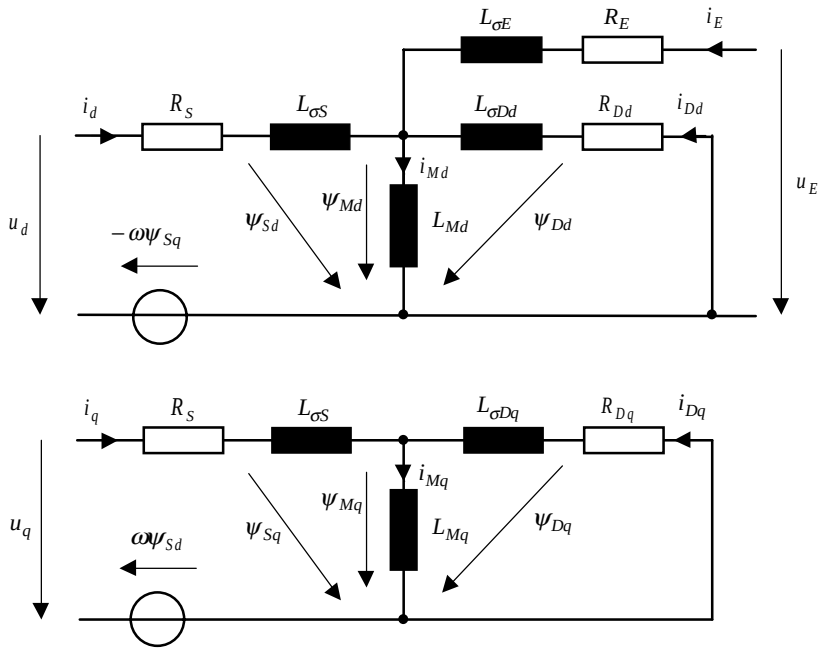

Fig. 5: Equivalent circuit diagram of the synchronous motor in the *d/q* reference frame

The mutual flux vector ψ_M spans a third reference frame, the *m/l* frame that is used for control purposes, see Fig. 4. The angle δ between the *d* and the *m* axes is the torque angle. The *m/l* frame is advantageous to calculate the motor torque as

$$T = \tfrac{3}{2} n_p \left(\psi_{Sd} i_q - \psi_{Sq} i_d \right) = \tfrac{3}{2} n_p \psi_M i_l ,$$

where n_p is the number of pole pairs.

Fig. 6: View on the uncoupled motor shaft.

Motor Control Structure

An overview of the control structure is given in Fig. 7. The components will be explained in the following sections.

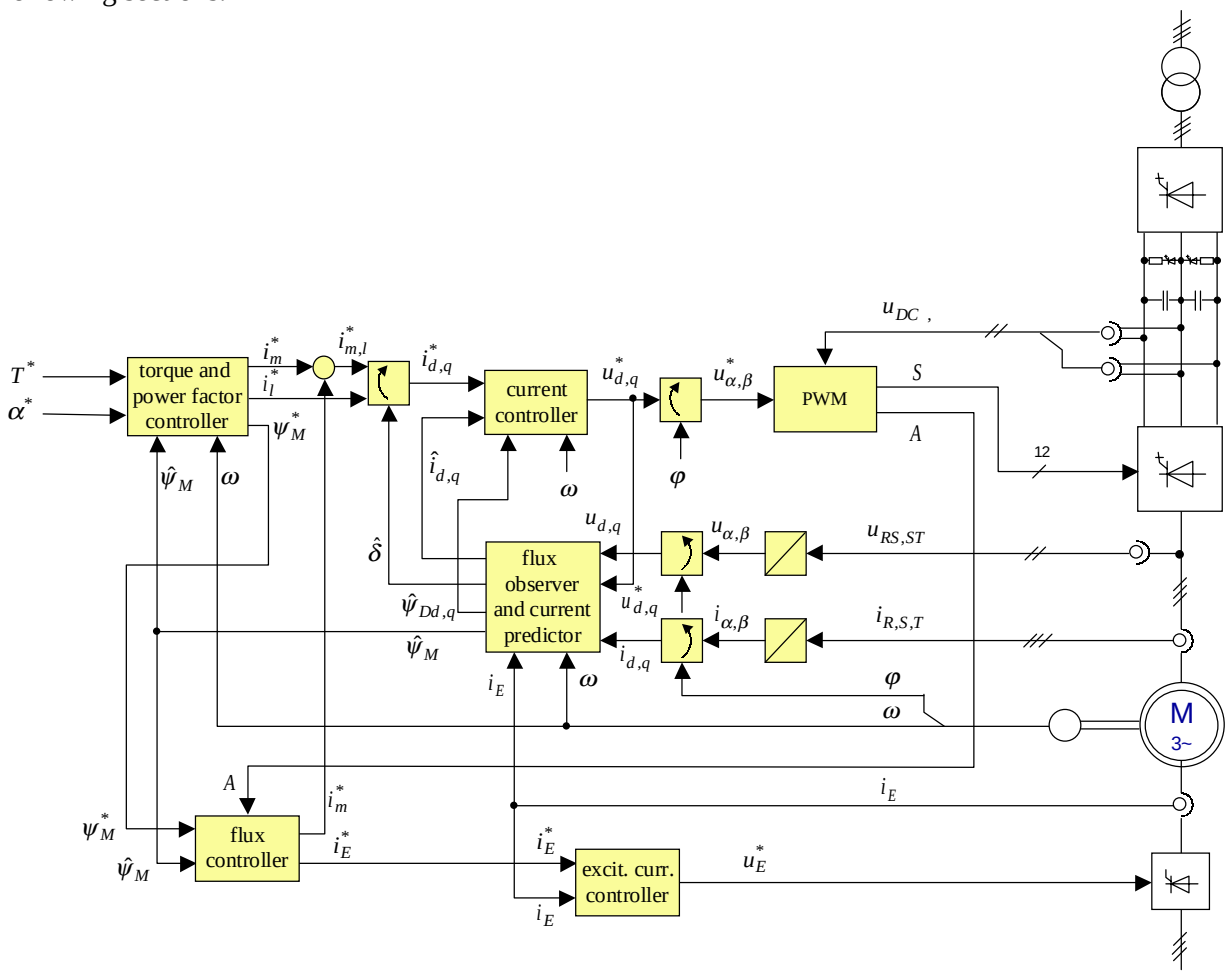

Fig. 7: Motor control structure.

Torque and Power Factor Controller

Depending on the torque demanded by the process control, the controller calculates a current demand i_l^* using the torque equation (as mentioned in the Section Motor Model) with the flux estimate $\hat{\psi}_M$. The demand i_{m1}^* is used to adjust the power factor of the motor. Additionally, a suitable set point ψ_M^* of the mutual flux is calculated depending on the speed and the demands of torque and power factor.

Flux Controller and Excitation Current Controller

The mutual flux is regulated by a closed-loop controller, again using the estimate of the flux observer $\hat{\psi}_M$. A supervision of the modulation depth A is also included in this block so that the voltage is prevented from getting completely saturated. The controller sets the demands for the excitation current i_E, which itself is controlled by an inner excitation current controller. A supporting additional control action i_{m2}^* is used by the flux controller for rapid flux changes as it is necessary during fast acceleration. During steady state, this additional signal is zero, so that the power factor is not impaired.

Stator Current Controller

The controller of the stator currents operates in the orthogonal *d/q* reference frame. Because the demands of the torque and flux controller are given in the *m/l* reference frame, a rotational transform is necessary first, which is carried out by the estimate $\hat{\delta}$ of the torque angle, i. e. the angle between the *d* and *m* axes.

A careful discrete-time design of the current controller is necessary in order to handle the relatively large sampling periods. Approaching maximum speed, only 12 samples per fundamental are available. As the sampling times are varied in order to synchronize switching and fundamental frequencies, the controllers need to cope with variations and even step-wise changes of the sampling frequency (cf. pulse width modulation section).

Fig. 8 and Fig. 9 show step responses of the i_l component, which is proportional to the torque. If sufficient voltage is available (lower speed range), the torque rise time is in the range of 5 ms, which are only 2 to 3 control samples. Even in the flux weakening range, the torque rise time is, depending on the step height, 10 to 30 ms.

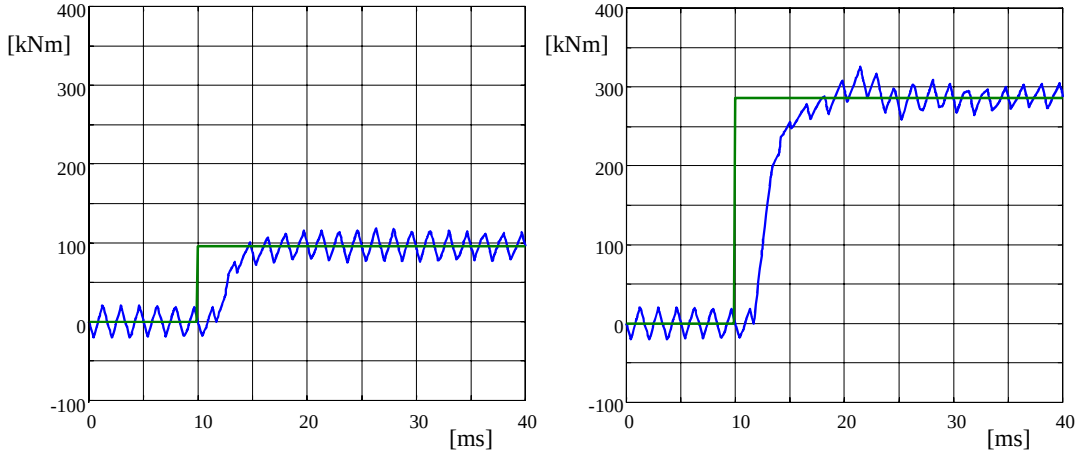

Fig. 8: Torque step-response, which is proportional to i_l step response, at 6Hz (50% of rated speed) from a simulation run.

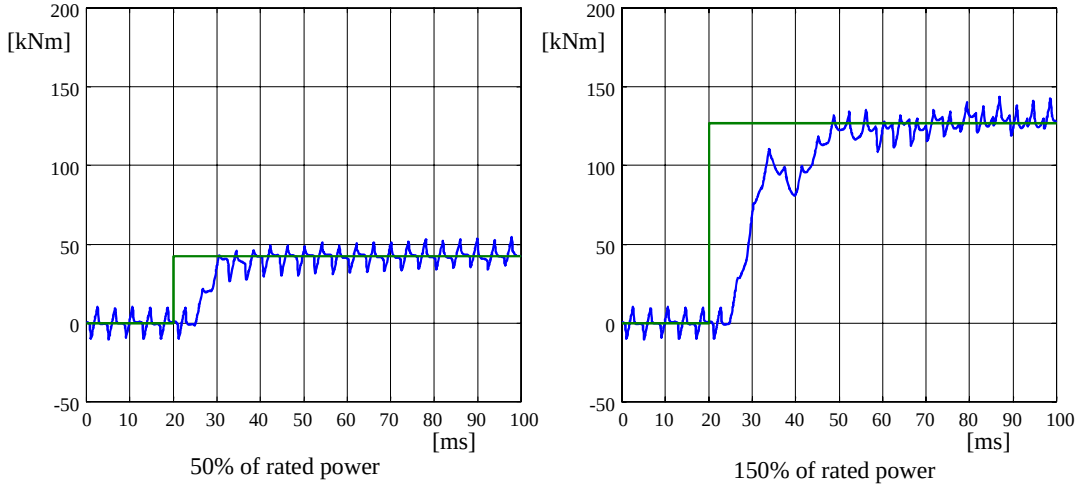

Fig. 9: Torque step-response at 41.3 Hz (225% of rated speed, i.e. max. speed) from a simulation run.

Flux Observer and Current Predictor

The flux observer has the task of estimating the non-measurable states of the motor, namely the magnetic fluxes. A Kalman filter-type observer similar to the one described for an induction motor [4], [5] has been employed. The complete state-space model of the equivalent circuit diagram shown in Fig. 5 is of order five. However, a reduced-order observer has been applied by treating the excitation current i_E not as an independent state to be estimated but as a given input to the remaining forth-order system. The observer provides all the estimates like the magnitude of the mutual flux $\hat{\psi}_M$, the damper flux vector $\hat{\psi}_{Dd,q}$, and also an estimated torque angle $\hat{\delta}$ that are needed in the other control modules.

With a minimum of additional effort, the flux observer can easily operate as a one-step ahead predictor. That is very valuable to compensate for the computational delay in the control loop, which is one sampling step. Thus, the current controller can be supplied with one-step ahead predictions of actual current values.

Pulse Width Modulation and DC Link Balancing

The well-known vector modulation has been applied as pulse width modulation technique. Shortly summarized, for a demanded voltage vector, three adjacent elementary voltage vectors have to be chosen and appropriate time ratios have to be calculated so that the resulting actual voltage, averaged over the considered sampling period, is exactly equal to the demanded voltage. This concept looks rather simple, but a closer inspection shows that several constraints have to be taken into account:

High power GTO thyristors, like those applied in the described VDM7000 converter, only allow a rather low switching frequency in order to achieve high efficiency. As it can be seen from the state transition diagram in Fig. 10, even transitions between neighboring states may require two switching actions, in which case there is no direct line between them. If the sequence of states is not chosen carefully, the resulting switching frequency may be unnecessarily high.

Each of the inner elementary voltage vectors can be realized by two different converter states (redundant states), the zero voltage vector even by three. The redundant states differ in charging (or discharging, resp.) of the DC link capacitors. So it is clear that the redundant states cannot be arbitrarily chosen, but a well thought-out sequence of these redundant states is necessary for balancing of the DC link.

Here, it is *not* applicable to exchange the selected redundant states at run-time in order to compensate for an acute DC link imbalance. Because of the low switching frequency, the exchange of only one redundant state would even exaggerate the DC link imbalance to the other direction. Run-time DC link balancing is done here by fine shifts of the pulse edges after their calculation by the vector modulation.

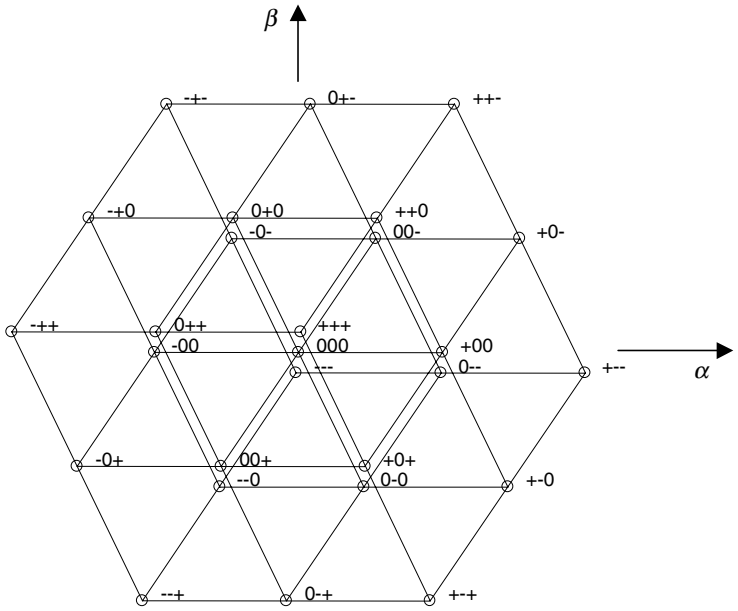

Fig. 10: Transition graph of the switching states of a three-level converter as projection in the orthogonal α/β plane. In order to better show the redundant states, the projection has been carried out slightly oblique. The triples of symbols +, 0 or – indicate connections to the upper, middle or lower DC link potential (cf. Fig. 2) for each of the three phases. A line between two states indicates that only one switching action is required to change from one state to the other.

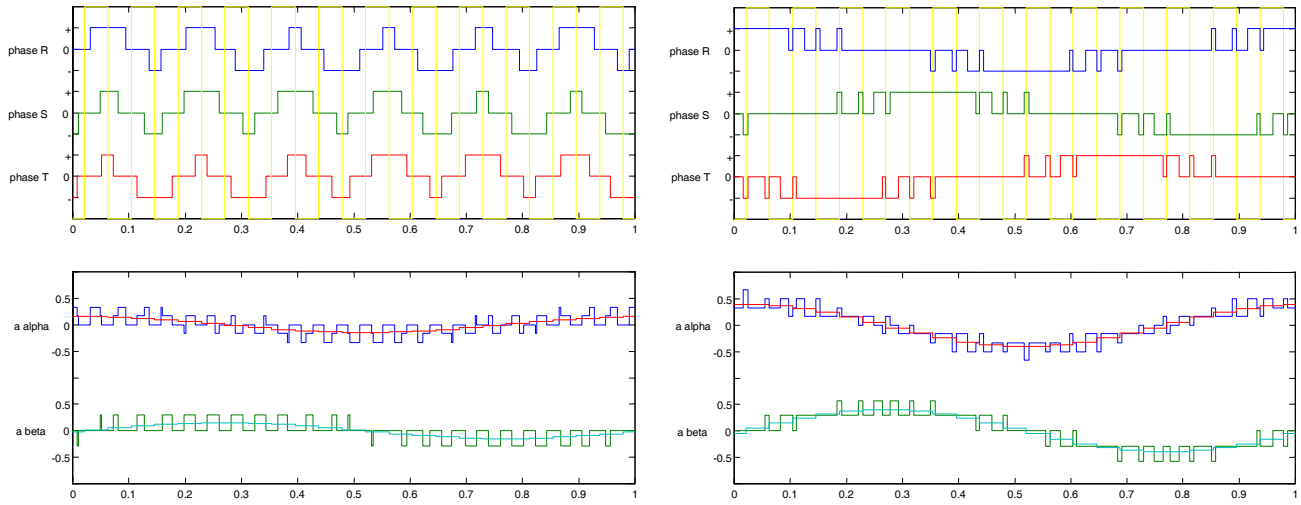

Fig. 11: Pulse patterns Type 1 with 26% modulation depth (left diagram) and Type 2 with 69% modulation depth (right diagram), both types are shown with 24 samples per fundamental period.

Depending on the fundamental frequency and the modulation depth, several types of pulse patterns are necessary. Two of them are depicted as examples in Fig. 11.

For lower fundamental frequencies, the switching frequency is fixed and asynchronous. However, a switching frequency reduction near standstill is applicable in order to reduce losses. For higher speed operation, a synchronization of switching and fundamental frequencies is necessary in order to avoid beating effects. During synchronized pulsing, the number of pulses per fundamental n_p and the number of samples n_s are integers. Because the regular sampling method is applied, which uses an identical sampling period for the controller and the vector modulation, the synchronization between

fundamental and switching frequency also results in varying sampling periods. Fig. 11 shows the scheduling scheme of asynchronous and synchronous pulsing and the usage of the pulse pattern types versus fundamental frequency. The pattern types and the numbers of samples are chosen not to exceed the allowed maximum switching frequency of 150 Hz. As it can bee seen from this diagram, the sampling period T_s varies in the range of 1.67 up to 3.6 ms. All control modules have to consider this variation and must be capable to handle even step-wise changes of the sampling frequency without causing any transient response.

The pulse pattern Type 2 is also applied to the line-side PWM with 12 samples per period, which results in a switching frequency of 150 Hz.

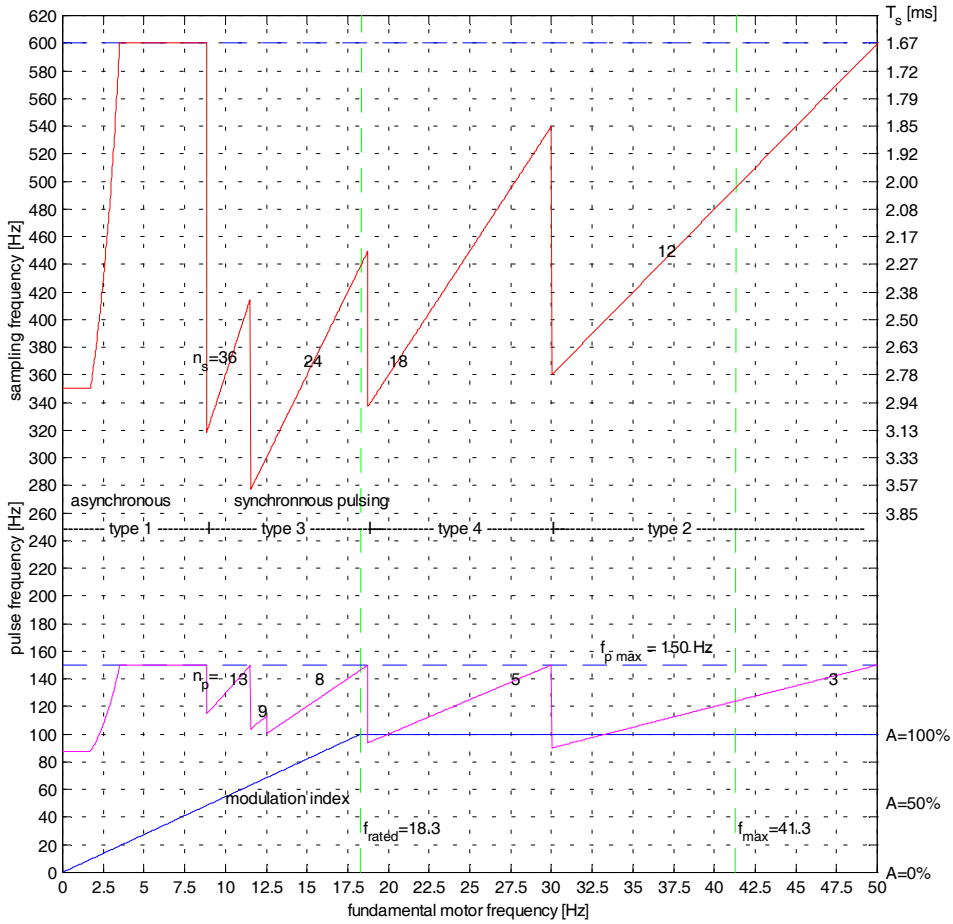

Fig. 12: Chart of pulse patterns and their resulting switching and sampling frequencies vs. fundamental frequency.

Controller Equipment

The converter control has been realized with Alstom's Power Electronic Controller System (PEC), which is typically applied for medium or large power converters. The system consists of various components as shown in Fig. 13. The converter-related control algorithms, like the line-side and motor-side controller parts, are implemented in C programming language on the Controller Interface Board (CIB). The CIB is equipped with a TMS 320C44-60 signal processor that provides 32 bit floating point arithmetic. If necessary, complex control algorithms can be distributed to several CIB boards, which exchange data via fast CIB to CIB communication channels or more slowly via the VME bus. By this architecture, the PEC system can be tailored to the needs of any converter system.

The I/O handling, the generation of the firing commands, and time critical converter protection functions are performed by the Power Interface Boards (PIB). The Local Interface Board (LIB) provides additional I/O for the speed and position sensors. The switching of each single thyristor including supervision and health monitoring is done by the Valve Interface Boards (VIB). The PIB and VIB components are positioned within the converter racks while the CIB board is located distanced from the converter in a separate controller rack, Fig. 14. The components are connected by optic fibers, which ensures best electromagnetic compatibility. Optic fibers are also a safety feature, because they allow complete galvanic isolation of the controller from the converter. Additionally, the commissioning effort regarding wiring is essentially reduced.

Communication with the process control is done via the VME bus. The process control is running on the COP 232, which is out of the scope of this paper.

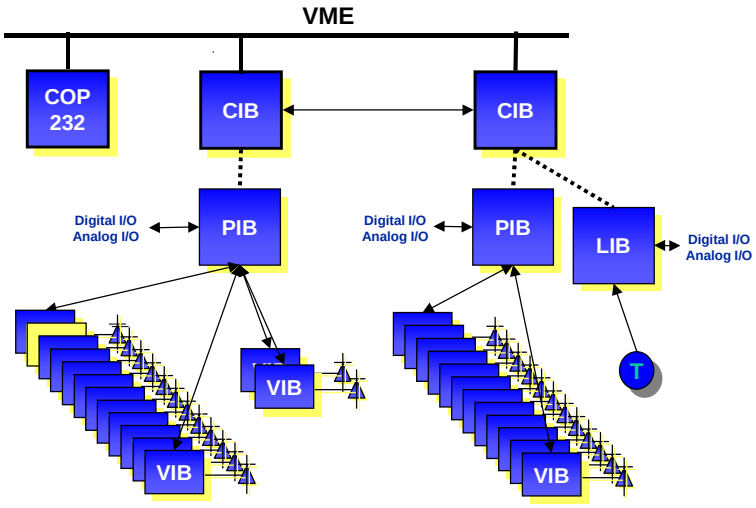

Fig. 13: Power Electronic Controller System (PEC).

Fig. 14: Controller rack.

Measurement Results

The following measurements have been made during commissioning while the motor was not yet coupled with the rolling mill. So, the load of the motor was only its own inertia. Unfortunately, coupling of the drive with the rolling mill will be done after the paper's deadline so that measurements at regular operation will be reported at the conference, but cannot be included in this paper.

Fig. 15 shows a slow acceleration at a small demand of 3.75 % of rated torque. The resulting speed and frequency, resp., shows a very good linear behavior.

The figure also shows the scheduling of the different pulse pattern types and the ranges of asynchronous and synchronous pulsing. During synchronous pulsing, n_s indicate the number of samples that are applied during a fundamental period. The sampling frequency is then appropriately adapted. As it can be seen from Fig. 15, the various pulse pattern changes do not affect the uniform acceleration.

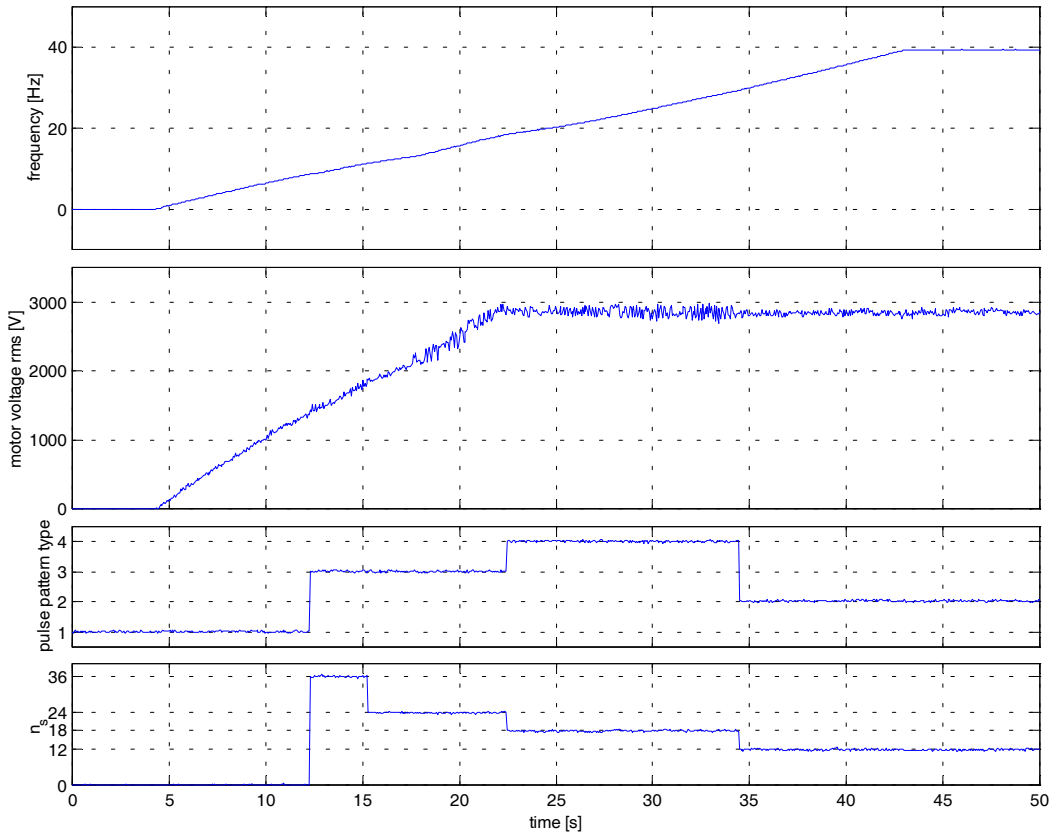

Fig. 15: Acceleration at a demand of 3.75 % of rated torque. The curves show the frequency, the motor voltage, the applied pulse pattern type, and the number of samples n_s per fundamental period during synchronous pulsing, $n_s = 0$ indicates asynchronous pulsing.

Acceleration and braking at a rated torque demand is shown in Fig. 16. The demanded torque can be realized even in the flux weakening range as long as the current limits are not reached.

Fig. 17 shows additional line and DC link signals during an acceleration and braking operation. The DC link voltage is kept close to its set point during the operation. During braking, the power is fed back into the line.

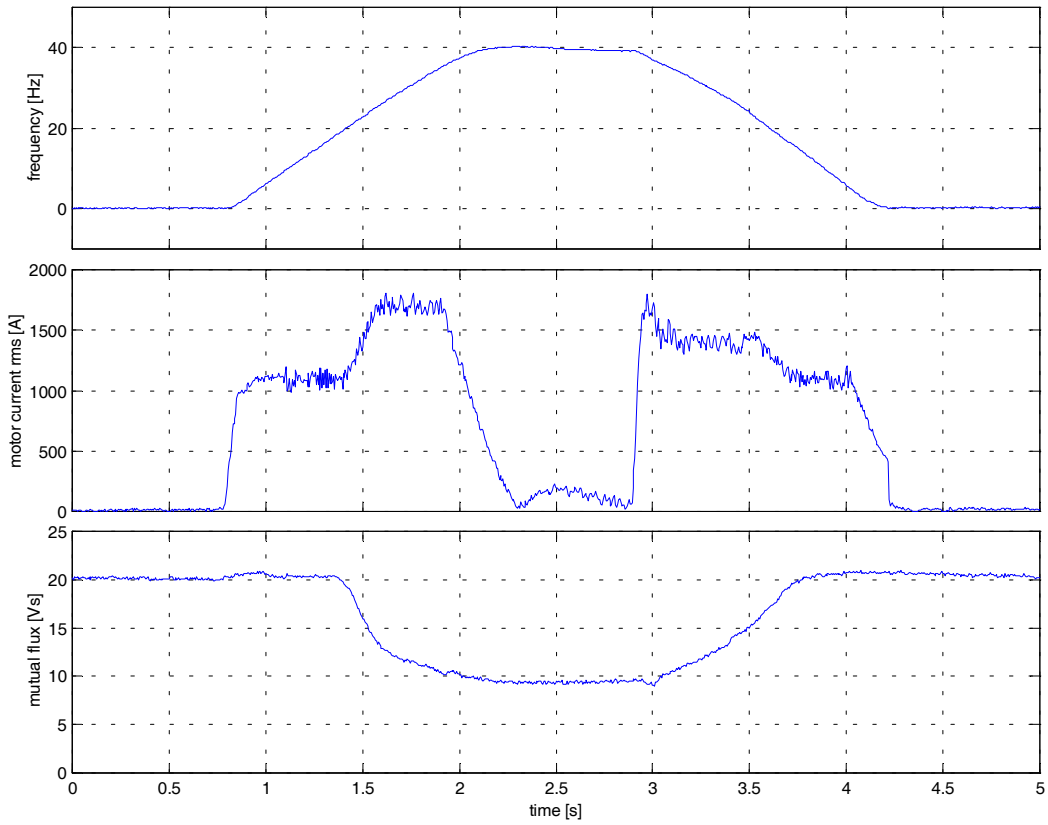

Fig. 16: Acceleration and braking at rated torque demand. The curves show the frequency, the motor current and the mutual flux vs. time.

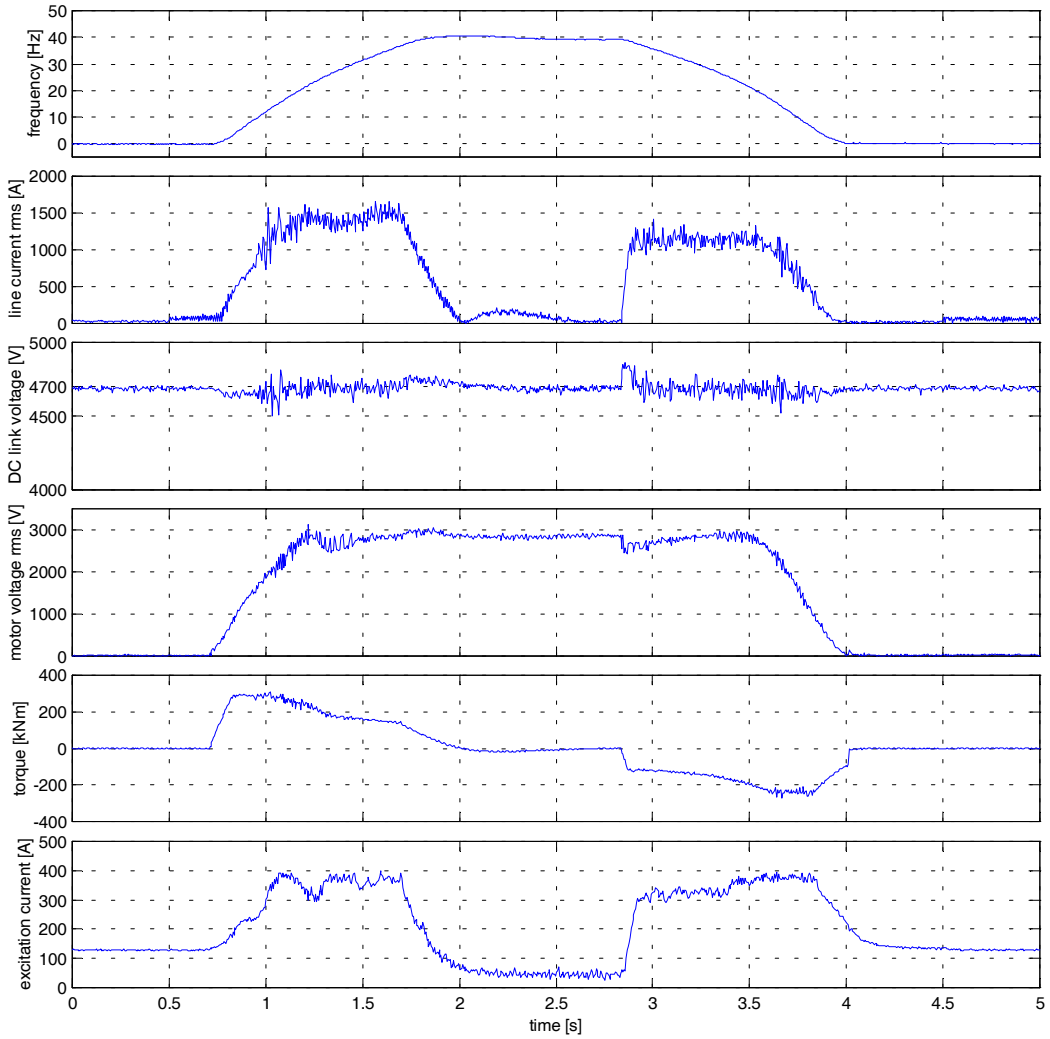

Fig. 17: Acceleration and braking at maximum motor current. The plots show the frequency, the magnitude of the line current vector, the DC link voltage, the motor voltage, the torque and the excitation current.

Conclusions

A high dynamic control has been presented for the high-power voltage source converter drive Alspa VDM 7000. The torque rise times of a few milliseconds are remarkable compared to the allowed switching frequency of only 150 Hz. This result was possible due to a consequent discrete-time design of the control system. Although switches between different pulse pattern types were necessary to cope with the low switching frequency, the torque's behavior is very smooth and regular. The system was put into operation for a main strip mill without problems. The tests have shown a reliable, trustworthy behavior.

With the present application, it has been shown that voltage source converters are a convincing option for cyclo converters even in the high power range.

Drive System Data

Converter

rated output voltage (RMS)	3.1 kV
rated output current (RMS)	1.7 kA
repetitive peak off-state voltage	4.5 kV
max. turn-off current	4.0 kA
max. switching frequency	150 Hz

Motor

rated/max. mechanical power	5.5 / 8.25 MW
rated voltage (RMS)	3.0 kV
rated current (RMS)	1.1 kA
rated/max. frequency	18.3 / 41.3 Hz
number of pole pairs	4

References

[1] Hermann Dicks, Jörg Janning. *Standardumrichter Typ BAUM für DB Energie*, Elektrische Bahnen, Vol. 98 (2000) No. 10, pp. 364-373

[2] Jörg Janning. *Regelung eines statischen Netzkupplungs-Umrichter zur Speisung des $16^2/_3$-Hz-Bahnstromnetzes aus dem 50-Hz-Landesnetz*, VDI Fortschrittberichte, Reihe 21, Nr. 235, 1997.

[3] Jörg Janning, Joachim Böcker, Kay Anbuhl, Marco Boni. *Netzkupplungsumrichter Jübek - Teil 2: Regelung*, Elektrische Bahnen, Nol. 93 (1995) No. 6, pp. 207-212

[4] Joachim Böcker. *Discrete-time model of an induction motor*, ETEP Vol. 1, No. 2, March/April 1991, pp.65-71

[5] Joachim Böcker, Jörg Janning. *Discrete-Time Flux Observer for PWM Inverter Fed Induction Motors*, Proc. EPE'91, Florence, 1991

[6] Joachim Böcker, Jörg Janning, Kay Anbuhl. *Realization of a High-Dynamic Discrete-Time Controller for PWM Inverter-Fed Induction Motor Drives*, Proc. EPE '93, Brighton, 1993